PROCEEDINGS OF SCIENCE

Fragmentation in e^+-e^- Collisions

David T. Kettler[*] **and Thomas A. Trainor**
University of Washington
E-mail:
`dkettler@npl.washington.edu`,`trainor@hausdorf.npl.washington.edu`

We analyze the energy scale dependence of fragmentation functions from e^+-e^- collisions using conventional momentum measures x_p and ξ_p and rapidity y. We find that replotting fragmentation functions on normalized rapidity u results in a compact form precisely represented by the beta distribution, its two parameters varying slowly and simply with parton energy scale Q. The resulting parameterization enables extrapolation of fragmentation functions to small Q in order to describe fragment distributions at low transverse momentum p_t in heavy ion collisions at RHIC.

Correlations and Fluctuations in Relativistic Nuclear Collisions
July 7-9 2006
Florence, Italy

PoS(CFRNC2006)003

---

[*] Speaker.

1. Introduction

Single-particle p_t spectra from p-p collisions and two-particle correlations from Au-Au collisions at RHIC measured with novel techniques have revealed *minijet* (low-Q^2 parton fragment) structure [1, 2, 3, 4, 5, 6, 7, 8, 9, 10, 11, 12]. Minijets are observed in nuclear collisions with *no jet hypothesis* (no high-p_t trigger-particle condition), providing access to minimum-bias parton scattering (no analysis constraint on parton momentum). Minijet correlations have been observed in p-p collisions for hadron p_t down to 0.35 GeV/c [12, 1]. Similar measurements in heavy ion collisions have revealed complex correlation structures related to parton dissipation in the QCD medium [2, 3] and medium response to parton stopping [6] which call into question the extent of equilibration.

Minijet correlations measured in p-p and heavy ion collisions at RHIC represent QCD in a *non*-perturbative regime: parton scattering and fragmentation at low Q^2. We want to connect those measurements in nuclear collisions to perturbative QCD (pQCD) *via* fragmentation measurements at larger Q^2. The context for fragmentation in nuclear collisions may be established by studying single-particle *fragmentation functions* (FFs) from e^+-e^- collisions, which provide precise access to the fragmentation process down to small parton and hadron momenta. Modification of parton scattering and fragmentation in heavy ion collisions compared to elementary collisions may then reveal the formation mechanism and properties of the QCD medium.

To establish the connection between the pQCD systematics of e^+-e^- FFs and minijets in nuclear collisions we must extend the FF phenomenology to low Q^2. In this paper we present a basis for extrapolating measured e^+-e^- FFs to small energy scale as preparation for extrapolation in nuclear collisions. We describe a new phenomenological analysis of FF data [13] which facilitates extrapolation to small parton energies where pQCD assumptions such as collinearity and factorization are not valid.

2. Analysis Method

The fragmentation function $D(x_p, Q^2)$ is a single-particle density $2dn/dx_p$ of hadron fragments on momentum fraction $x_p = p_{hadron}/p_{parton}$ produced by a *pair* of partons (dijet) with total energy Q ($Q^2 = -q^2$ is the negative invariant mass squared). At large x_p the distribution reflects energy conservation during parton splitting [14, 15]. At small x_p the shape is determined by quantum coherence of gluon emission [16, 17]. The FF data in this study are hadron distributions reported on momentum fraction x_p or logarithmic variable $\xi_p \equiv \ln(1/x_p)$. Distributions on x_p emphasize pQCD aspects of parton fragmentation at large p (*e.g.,* scaling violations). For non-pQCD effects ξ_p provides better access to the small-x_p (large-ξ_p) region.

This study focuses on low-Q^2 parton fragmentation dominated by fragments with small momenta. We therefore introduce rapidity y (well-behaved as $p \to 0$) as an alternative logarithmic momentum variable. In a frame where p is the only non-zero momentum component $y(p; m_0) = \ln[(E + p)/m_0]$, with $y \to \ln(2p/m_0)$ for $p \gg m_0$ and $\to p/m_0$ for $p \ll m_0$. m_0 may be a quark or hadron mass or energy scale Λ. For unidentified fragments we assign the pion mass $m_0 \to m_\pi$ to all hadrons. Given the limiting cases for y we note that $\ln(\sqrt{s}/m_0) \sim y(\sqrt{s}/2; m_0) \equiv y_{max}$, the parton rapidity (defined as the kinematic limit for fragment rapidities). Similarly, $Y(Q) = \ln(Q/\Lambda) \sim$

$y(Q/2;\Lambda)$ is a rapidity measure of the energy scale relative to a reference scale. We observe for FF data a lower limit y_{min} which may depend on fragment species and collision system (e.g., e^+-e^- *vs* p-$\overline{\text{p}}$).

From published data distributions on x_p or ξ_p for parton energy scale Q or CM energy $\sqrt{s}$ we extract fragment momenta p and calculate equivalent rapidities y (fragments) and y_{max} (partons). Data distributions on x_p or ξ_p are thereby transformed to distributions on y using appropriate Jacobians. Most e^+-e^- FFs plotted on normalized rapidity $u \equiv (y - y_{min})/(y_{max} - y_{min}) \approx 1 - \xi_p/Y$ have a particularly simple form described by the *beta distribution* [13]. The unit-normal beta distribution defined on $u \in [0,1]$ is $\beta(u;p,q) = u^{p-1}(1-u)^{q-1}/B(p,q)$, with parameters $p, q \geq 0$ and beta function $B(p,q) = \frac{\Gamma(p)\,\Gamma(q)}{\Gamma(p+q)}$.

3. Fragment distributions on momentum

The fragmentation functions in Figs. 1 and 2 were obtained from e^+-e^- collisions at three energy scales (CM energy $\sqrt{s}$ = Q = 14, 44 and 91.2 GeV) measured at PETRA [18] and LEP [16] for unidentified hadrons from unidentified partons. Those FFs are fiducial because of the exceptional data quality and fragment momentum coverage. In Fig. 1 (first panel) we plot FFs on momentum fraction x_p. Distributions on x_p emphasize the large-x_p (small-ξ_p) region where pQCD best describes the data, where the naïve parton model predicts 'scaling' or invariance of the parton distribution on energy scale Q. Distribution details in the small-x_p region (*e.g.*, below $x_p = 0.1$), where non-pQCD dominates and fragments are *most abundant*, are minimized in this format. The dashed line illustrates the exponential model sometimes used to characterize FFs on x_p.

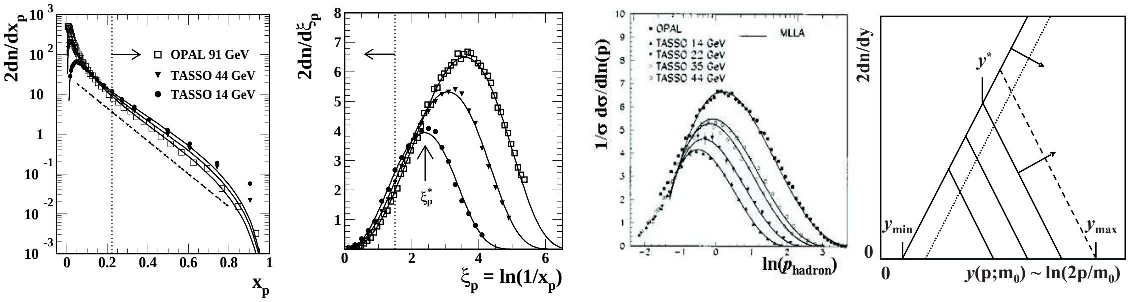

Figure 1: First panel: e^+-e^- fragmentation functions on fractional momentum $x_p = p_{\text{fragment}}/p_{\text{parton}}$ for three CM energies. The dashed line is an exponential reference. Second panel: The same fragmentation functions on logarithmic variable $\xi_p = \ln(1/x_p)$. The vertical dotted lines mark equivalent points on the two variables. The solid curves are determined by the parameterization from this analysis. Third panel: Distribution on $\ln(p_{hadron})$ from [16]. Fourth panel: Self-similar variation with energy of fragment distributions on y.

The vertical dotted line in the first panel corresponds to $\xi_p = 1.5$ in the second panel: only a small fraction of fragments (< 10%) fall above that point on x_p. FFs on ξ_p are *approximately* gaussian, with mode ξ_p^* and width predicted by pQCD. The fall-off at large ξ_p and maximum at ξ_p^* result from gluon coherence [16, 17]. FFs exhibit systematic *scaling violations* (Q dependence) described by the DGLAP evolution equations (*cf.* Sec. 6) [14, 15]. To study scaling violations FFs on x_p are parameterized by a model function such as $D(x,Q^2) = N x^{\alpha}(1-x)^{\beta}(1+\gamma/x)$, where

PoS(CFRNC2006)003

the four parameters depend on parton type, hadron type and energy scale [19, 20]. The solid curves in the first two panels are beta distributions $\beta(u;p,q)$ determined by the systematic trends of parameters (p,q) plotted in Fig. 4 (third panel) and transformed from normalized rapidity u to x_p, ξ_p or y with appropriate Jacobians.

The third panel shows FFs plotted on $\ln(p)$ [16]. The solid curves are MLLA pQCD predictions [22]. The general shape and evolution of FFs with p_{parton} on (y, y_{max}) is sketched in the fourth panel. The trend corresponds to the DLA [21] with angular ordering and gluon coherence (modified leading log approximation or MLLA [22])

4. Precision model function

Fragmentation functions plotted on ξ_p coincide at the kinematic limit $\xi_p = 0$ corresponding to the parton momentum. An approximation to 'scaling' or energy-scale independence is expected at small ξ_p (large x_p). Another form of scaling, at large ξ_p, can be explored by plotting distributions on rapidity y. In Fig. 2 (first panel) we observe that the FFs for three energies plotted on y have a common low-momentum limit $y_{min} \sim 0.35$ (vertical line). That alignment is possible because y has the well-defined limiting value 0 as momentum $p \to 0$. Each data FF is terminated at the upper end by its kinematic limit $y_{max} = y(\sqrt{s}/2; m_0)$ (vertical lines) corresponding to $\xi_p = 0$ in Fig. 1. The distribution maxima increase monotonically with collision (parton) energy. The FFs in the first panel illustrate the self-similarity sketched in Fig. 1 (fourth panel) and confirm an expectation for DLA scaling: fragmentation at small y should be nearly independent of the leading-parton momentum.

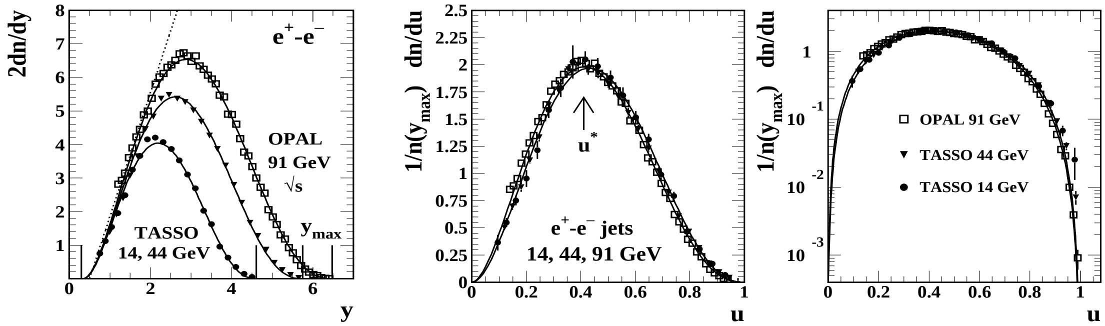

Figure 2: Fragmentation functions on rapidity y for e^+-e^- collisions (left panel). Fragmentation functions plotted on normalized rapidity u in linear (left panel) and semi-log (right panel) formats. The data distributions have been normalized by the corresponding di-jet multiplicity at each energy (lower solid curves in determined by parameters (p,q). The data for three energies are plotted, but the curves for only 14 and 91 GeV are plotted to provide visible separation.

In Fig. 2 (right panels) we plot the three fiducial FFs transformed to $1/n(y_{max})\,dn/du \equiv g(u, y_{max})$. Expectations of approximate energy scaling at large x_p and a different form of scaling (gluon coherence) at small x_p seem to require conflicting plotting strategies on ξ_p and y. However, both forms can be accommodated by introducing normalized rapidity $u \equiv (y - y_{min})/(y_{max} - y_{min}) \in [0,1]$. FFs from e^+-e^- collisions can be factored as $D(u, y_{max}) = 2n(y_{max})\, g(u, y_{max})$, with dijet multiplicity $2n(y_{max})$ (*cf.* Fig. 4) and unit-normal form factor $g(u, y_{max})$. Multiplicity $2n(y_{max})$ can be obtained by integrating data FFs, but also from the *shape* of $g(u, y_{max})$ (*cf.* Sec. 6.1). We observe that the $g(u, y_{max})$ are nearly invariant over a large energy scale interval, and the beta distribution provides an excellent description over all fragment momenta.

5. Identified fragments and partons

In Fig. 3 we show data $g(u, y_{max})$ and best-fit model $\beta(u; p, q)$ for identified charged pions $\pi^\pm$ (first panel) and kaons $K^\pm$ (second panel) at 10 GeV [23] and 91 GeV [24]. Parton rapidity y_{max} is calculated with the identified hadron fragment mass. The pion FFs have widths similar to unidentified hadrons, but the peak modes are significantly lower (0.38 *vs* 0.41 at 91 GeV). The kaon peak modes are comparable to unidentified hadrons but the peak width at higher energy is significantly larger. The kaon FF shape seems to converge on the pion distribution at lower energy. The apparent merging of quark flavors at 10 GeV is consistent with convergence of the gluon and quark FFs at lower energy, indicated by the multiplicity and (p, q) trends in Fig. 4.

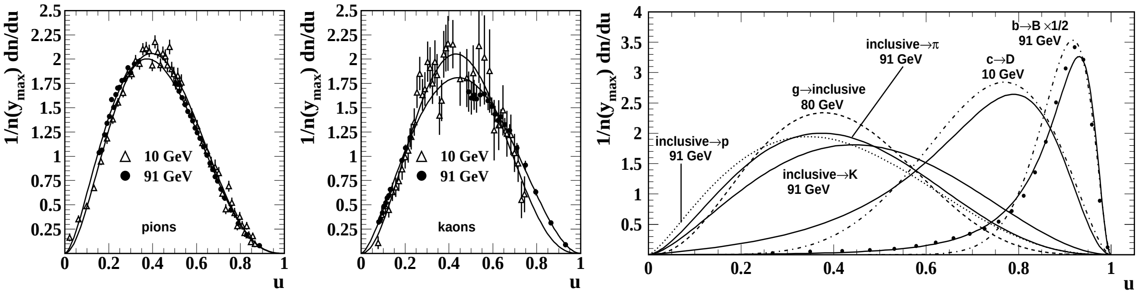

Figure 3: Fragmentation functions for two CM energies and for pion (left panel) and kaon (right panel) fragments plotted on normalized rapidity u. Distributions on u for several quark/meson flavor combinations, showing evolution of the $g(u, y_{max})$ shape with quark/meson mass. The c → D data are from [26], and the b → B data are from [25]. The energies are dijet energies.

In Fig. 3 (third panel) we summarize FF data and models for several fragment and parton types. The pion, kaon and proton FFs are beta distribution fits to 91 GeV identified-fragment data (as in the first two panels). The gluon FF is the beta distribution defined at 80 GeV by (p, q) systematics in Fig. 4 (third panel, consistent with fits to gluon data FFs). The solid dots are b → B data [25] compared to a best-fit beta distribution (dash-dot curve) and theory (solid curve). Low-statistics c → D data [26] are summarized by a best-fit beta distribution (dash-dot curve) and theory (solid curve).

The two solid curves on the right are from a theoretical treatment of heavy-quark fragmentation [27]. The agreement of $D_b^B(u)$ (right-most solid curve) with b-quark data (solid points) [25] is good. The dash-dot curve is the best-fit beta distribution with $(p, q) = (23, 3)$ which does not describe the $b \rightarrow B$ data well. The solid curve for $c \rightarrow D$ is $D_c^D(u)$ from the heavy-quark theory treatment, with $\varepsilon_Q = 0.57/m_c^2 = 0.29$ and $m_c \sim 1.4$ GeV/c^2. The associated dash-dot curve, a beta distribution with $(p, q) = (7.0, 2.8)$, best describes the data from [26]. Both curves are consistent with the data, but errors are large below the FF peak mode.

To summarize the flavor dependence: the beta distribution describes the FF data for identified light quarks and gluons fragmenting to light mesons or baryons very well. The FF modes for a given parton energy increase monotonically with increasing meson and parton mass. However, the proton FF mode for udsc (light quark) jets is lower than the inclusive hadron mode for gluon jets, and the FF is significantly broader. The hadron mass alone is not a determining factor. The kaon FF shows the effect of the heavier s-quark mass, consistent with the trend for charm and bottom quarks.

6. Energy systematics of fragmentation functions

We have combined fiducial FF data and dijet multiplicity data to determine the energy dependence of β parameters (p,q) for quark and gluon jets. Fits to data $g(u,y_{max})$ with model $\beta(u;p,q)$ determine (p,q) over a limited energy range which constrains the parameterized curves $(p(y_{max}),q(y_{max}))$. Fits to $2n(y_{max})$ data over a broader energy range *via* the $\langle x_E \rangle$ integral (sum rule) of $\beta(u;p,q)$ also constrain the parameterizations, especially important at low energy where there are no FF data. The resulting (p,q) energy trends efficiently represent all e^+-e^- light-quark and gluon FFs and provide a basis for extrapolating FFs to low Q^2.

6.1 Dijet multiplicities from $\beta(u;p,q)$ shapes

Dijet multiplicity $2n$ can be obtained directly by integrating published FF data. However, there is a correspondence between $2n(y_{max})$ and the *shape* of data FF $g(u;y_{max})$ or fitted model function $\beta(u;p,q)$ determined by parameters $[p(y_{max}),q(y_{max})]$. For inclusive *charged* fragments we obtain the relation $2n(y_{max}) = 1.18/\int_0^1 du\, x_E(u,y_{max})\beta(u;p,q)$ (based on the energy sum rule [28]) which we use to relate energy trends of FF shape parameters (p,q) to fragment multiplicities. Measured multiplicities (*vs* parton energy) thus provide constraints on the energy dependence of FF parameters (p,q), even in energy intervals where there are no FF data.

Fig. 4 (left panels) shows dijet multiplicities $2n$ for g-g and q-$\overline{\text{q}}$ parton pairs. Data for gluon jets were obtained from CDF (closed triangles) [29], CLEO (open triangles) [30], OPAL 'jet-boost' algorithm (open circles) [31] and OPAL inclusive (star) [32]. Data for quark jets were obtained from a compilation (Table 6 in [33]). The large points labeled π and K are multiplicities from fits to identified fragment data [23, 24, 34] plotted with the indicated multipliers. The hatched regions represent the domain of low-Q^2 partons which motivated this study.

The solid curves in Fig. 4 (left panels) are multiplicity trends derived from the (p,q) parameters in the third panel using the energy sum rule. The (p,q) energy parameterizations are adjusted to fit the multiplicity data but are constrained by (p,q) values derived from fits to the fiducial FFs. The resulting (p,q) energy dependence is described in the next subsection.

6.2 Energy dependence of $\beta(u;p,q)$ parameters

Fig. 4 (third panel) shows the (p,q) energy dependence which produced the quark and gluon jet multiplicities (solid curves) in Fig. 4 (left panels) and the solid curves compared to fiducial FFs in Figs. 1 and 2. The $(p.q)$ curves precisely summarize the energy dependence of light-quark and gluon fragmentation to unidentified hadrons in e^+-e^- collisions. The vertical dotted lines mark the limits of multiplicity measurements, and the vertical dash-dot lines mark the limits of measured FFs used in this analysis. The ten solid points represent the fiducial FFs (dominated by quark jets). The open squares represent a fit to a single gluon FF which constrains $(p_{\text{g}},q_{\text{g}})$.

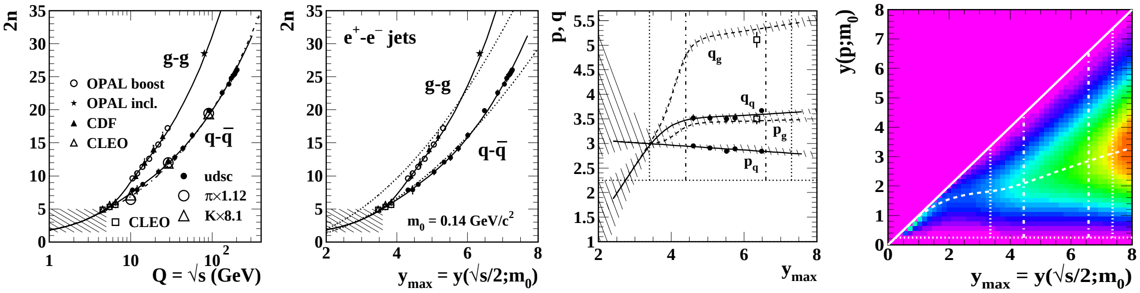

Figure 4: Left panels: Dijet charged-particle multiplicity *vs* energy scale Q (dijet energy) plotted in a conventional format (first panel) and *vs* parton rapidity assuming the pion mass (second panel). The solid curves are quark and gluon dijet multiplicities $2n_\mathrm{q}$ and $2n_\mathrm{g}$ obtained from the (p,q) parameterizations in third panel. The dash-dot curve in the first panel is from a 3NLO pQCD expression. The udsc quark-jet multiplicities for unidentified hadrons (solid dots) are taken from a survey in [33]. Third panel: Beta-distribution parameters $(p_\mathrm{q},q_\mathrm{q})$ and $(q_\mathrm{g},p_\mathrm{g})$ respectively for light-quark (solid) and gluon (dashed) jets and corresponding gluon-to-quark-jet multiplicity ratio r *vs* parton rapidity y_{max}. Fourth panel: Joint fragment distribution $D(y,y_{max})$ on fragment and parton rapidities for inclusive partons ($\sim$ udsc quarks) and inclusive hadrons. Fragmentation functions are vertical slices (conditional distributions) from the joint distribution.

Above $y_{max} = 4.5$ (left dash-dot line) the (p,q) vary slowly and linearly with increasing energy scale. That energy dependence implies a slight reduction of FF modes with increasing energy, consistent with the fiducial FFs in this study (*e.g.,* Fig. 2, right panels). Below $y_{max} = 4.5$ ($Q \sim 10$ GeV) the (p,q) change rapidly. The multiplicity data, especially the CLEO data, require a sharp drop in q in that energy interval for both quarks and gluons. The convergence of the quark and gluon (p,q) at the energy scale defined by the left dotted line (5 GeV) is again required by the CLEO data.

6.3 Fragmentation functions on (y,y_{max})

We use the parameterized beta distribution to construct a 2D fragment distribution on (y,y_{max}) as follows. $\beta(u;p,q)$ describes the shapes of FFs over a broad Q^2 interval. The beta distribution in turn determines multiplicity $n(y_{max})$ *via* the energy sum rule over the same range. We combine the two factors to form $D(y,y_{max}) = 2n(y_{max})\,\beta[u(y,y_{min},y_{max});p(y_{max}),q(y_{max})]$. In Fig. 4 (fourth panel) we plot $D(y,y_{max})$. The vertical dotted and dash-dot lines mark the same energy limits, as in the third panel. The dashed curve is a ‘locus of modes’ (positions of maxima) of conditional distributions on y for given y_{max}. The horizontal dotted line denotes y_{min}, and $y_{max} = 8$ corresponds to $\sqrt{s} \sim 400$ GeV. That 2D fragment density provides the basis for extrapolating FFs down to $Q \sim 1$ GeV ($y_{max} \sim 2$).

7. Comparisons with pQCD

The energy dependence of FF statistics predicted by pQCD [28, 35, 36, 37] can be compared to peak statistics inferred from our (p,q) parameterization of $\beta(u;p,q)$. In Fig. 5 (first panel) we compare beta distributions and data for two energies on normalized rapidity u using the parameters described above with corresponding MLLA gaussians (normalized to unit integral). The gaussian tails do not describe the data. Our parameterized model is consistent with pQCD predictions at larger Q^2, and the beta distributions (solid curves) demonstrate good sensitivity to small but meaningful systematic variations with energy of the FF data.

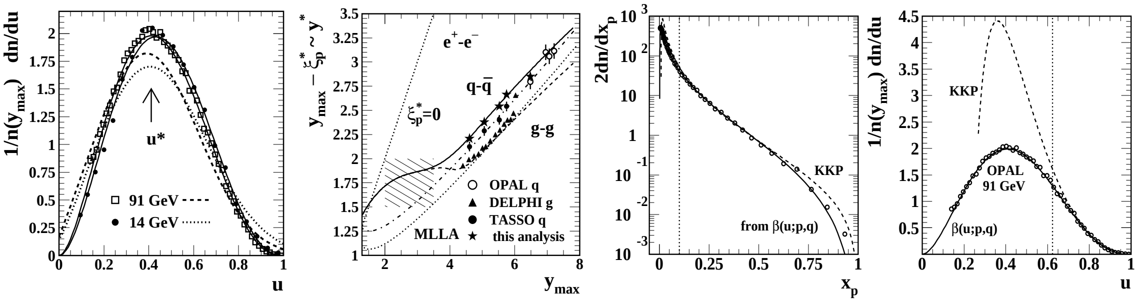

Figure 5: First panel: Comparison of fragmentation-function modes *vs* parton rapidity from quark and gluon data (points) with 'locus of modes' trends (solid and dashed curves) derived from (p,q) energy systematics in (left panel) and from the MLLA (dash-dot and dotted curves). Second panel: Comparison at two energies of FF data, beta distributions on u and MLLA gaussians suitably transformed to u. Third panel: Beta distribution (solid) and KKP FF (dashed) curves compared to OPAL 91 GeV data points (open circles) on linear momentum variable x_p. Fourth panel: The same curves and data transformed to normalized rapidity u. The vertical dotted lines both correspond to $x_p = 0.1$.

In Fig. 5 (second panel) we show measured modes ξ_p^* in the form $y_{max} - \xi_p^* \sim y^*$ *vs* y_{max} for eight quark-jet and fourteen gluon-jet energies [16, 18, 37]. The solid curve $y^*(y_{max})$ for quark jets from our (p,q) parameterization is the same as the dashed curve in Fig. 4 (fourth panel). The five stars are obtained from our fits to the fiducial FFs (compare to peak modes in Fig. 2 first panel). The MLLA prediction for inclusive jets is plotted as the dash-dot curve in the second panel. The MLLA curve diverges from the $(p_\mathrm{q}, q_\mathrm{q})$ parameterization (solid curve) in the region of interest for study of low-Q^2 partons (hatched area). We can also obtain a mode prediction for gluon jets [36, 37]. The corresponding dotted curve in the second panel agrees fairly well above $y_{max} = 4.5$ ($Q \sim 12$ GeV) with the gluon y^* trend (dashed curve) obtained from parameters $(p_\mathrm{g}, q_\mathrm{g})$ in Fig. 4 (third panel). Data from [37] for FF modes from gluon jets plotted as solid triangles are well described by the dashed curve obtained from our (p,q) energy systematics and by the MLLA prediction.

In Fig. 5 (right panels) we compare fiducial FF data to the beta-distribution description from our analysis and a pQCD model FF (KKP) obtained from a conventional scaling-violations analysis using the DGLAP equations [20] (defined by 14 parameters for each parton-hadron combination). Fig. 5 (third panel) shows the OPAL 91 GeV FF data from Fig. 2 with the KKP FF (dashed curve) and the FF from this analysis (solid curve). With the exception of a small deviation at large x_p the agreement on x_p appears to be good. Fig. 5 (fourth panel) shows the same distributions on normalized rapidity u. The KKP FF deviates strongly from data below $u = 0.7$ and accurately represents less than 10% of the fragments at 91 GeV. The vertical dotted line in each panel shows the intended region of validity ($x_p > 0.1$) of the KKP and similar FFs. The FF from our analysis accurately describes the data on x_p over six orders of magnitude and extrapolates the full data distribution down to zero momentum.

8. Scaling violations

Scaling violations [27]—variation of parton distribution functions (PDFs) and FFs with energy scale—are described by the DGLAP equations [14, 15]. Scaling violations of measured FFs can be used to determine α_s [38] and to test the predicted values of QCD color factors C_A and C_F [37]. We use our FF parameterization to describe scaling violations on conventional momentum/energy fractions and on rapidity variables .

8.1 Scaling violations on (x, Q^2)

The DGLAP equations [14, 15] are defined to leading order (LO) by

$$\frac{dD_b(x,s)}{d\ln s} = \frac{\alpha_s(s)}{2\pi}\sum_a \int_x^1 \frac{dz}{z} P_{ab}(z)\, D_a(x/z,s). \tag{8.1}$$

$P_{ab}(z)$ are the Altarelli-Parisi splitting functions [15], and a, b denote parton combinations. Scaling violations are determined from FFs parameterized at several energy scales s $(= Q^2)$ with a model function such as $D(x,s) = N\, x^{\alpha}\,(1-x)^{\beta}\,(1+\gamma/x)$ [19, 20, 37, 39]. Such parameterizations can be quite extensive. The KKP parameterization [20] employs 14 parameters for each parton-hadron combination, the energy dependence of each of $(N, \alpha, \beta, \gamma)$ being described by several polynomial coefficients. The parameters are determined by using the DGLAP equations to evolve the model FFs across energy scales, varying $(N, \alpha, \beta, \gamma)$ with energy to best fit the data and emphasizing the region $x > 0.1$ where pQCD is most applicable (*cf.* Fig. 5 – third panel).

To illustrate scaling violations we transform parameterized joint fragment distribution $D(y, y_{max})$ (Fig. 4 – fourth panel) to $D(x_E, Q^2) = p/(E\, x_E) D[y(x_E, Q), y_{max}(Q)]$. In Fig. 6 (first panel) we plot resulting conditional distributions $D(x_E, Q^2)$ for x_E = 0.02, 0.07, 0.15, 0.27, 0.41, 0.60, 0.81 *vs* $Q = m_0 \cosh(y_{max})$. The curves for both udsc jets (solid) and gluon jets (dashed) compare well with a data analysis shown in the second panel (x_E values are on the right) [40]. The general trends in the first panel agree with the conventional description of scaling violations but extend over a broader energy range than is usually obtained from data. The sharp falloffs at smaller Q and x_E occur at kinematic limits $\ln x_E \sim y_{min} - y_{max}$ defined by the dotted line in Fig. 4 (fourth panel).

The vertical dotted lines separate three regions. Region A ($Q = 1-5$ GeV) is dominated by non-perturbative effects but produces the majority of parton fragments in nuclear collisions and therefore requires a phenomenological characterization consistent with QCD theory. Extrapolating FF systematics into that region is the purpose of this study. Region B ($Q = 5-20$ GeV) is the transition region in which parton color emerges and fragmentation approaches a perturbative description. In the energy range above $Q = 20$ GeV parameters (p, q) vary weakly and linearly: fragmentation is fully perturbative. We conclude that much of the variation in the perturbative third region of Fig. 6 (first panel) is determined by phase-space acceptance variations with parton energy. The small linear variations of the (p, q) parameters in that region may provide more differential access to the parton cascade process. We therefore consider a modified form of the DGLAP equations.

8.2 Scaling violations on (y, y_{max})

In a different approach to scaling violations we introduce the *logarithmic derivative* [37] based on the relation between Mellin transforms of FFs and splitting functions. The DGLAP equations, written in terms of Mellin transforms $\hat{D}(w,s)$ (w is conjugate to x) [14], are represented by a simple

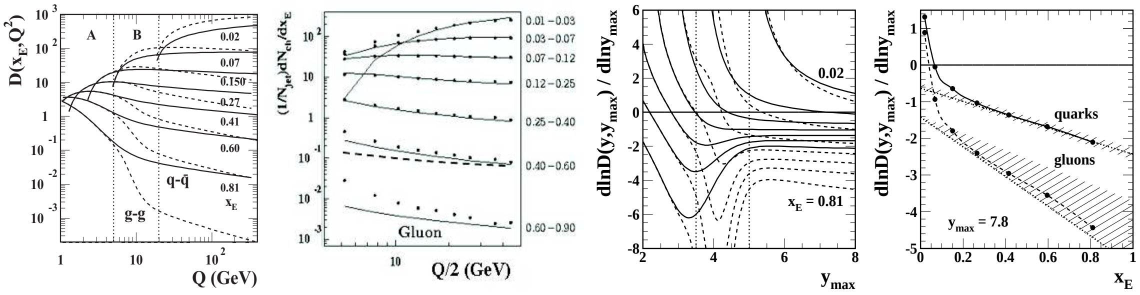

Figure 6: First panel: Scaling violations in a conventional format. Each curve is a conditional slice at fixed x_E from the distribution $2dn/dx_E(x_E, Q^2)$ suitably transformed from model function $2n(y_{max})\,\beta(u(y);p,q)$ in (second panel). Third panel: Scaling violations in the form of logarithmic derivatives of the distributions in (left panel). Solid curves represent udsc quark jets, dashed curves represent gluon jets. The near uniformity to the right of the dotted line ($Q = 20$ GeV) for larger x_E is notable. Fourth panel: Logarithmic derivatives for quark and gluon jets at $y_{max} = 7.8$ *vs* energy fraction $x_E = \cosh(y)/\cosh(y_{max})$.

matrix equation [15]. For the *non-singlet* case $\hat{D}_{\rm ns} = \hat{D}_{\rm q} - \hat{D}_{\bar{q}}$ the logarithmic derivative is

$$\frac{d\ln \hat{D}_{\rm ns}(w,s)}{d\ln s} = \frac{\alpha_s(s)}{2\pi}\hat{P}_{\rm qq}(w) \equiv \gamma_{qq}(w,s), \tag{8.2}$$

where $\hat{P}_{qq}(w)$ is the Mellin transform of splitting function $P_{qq}(z)$ for the process q → q(z) + g(1-z), with the respective momentum fractions, and $\gamma_{ab}(w,s)$ are the *anomalous dimensions* of QCD [41, 42]. Since $d\ln s \approx 2dy_{max}$ we multiply through by $2y_{max}$ and use the results of the previous subsection to obtain

$$\frac{d\ln \hat{D}_{\rm ns}(w,y_{max})}{d\ln y_{max}} = \frac{1}{\pi A}\,\hat{P}_{qq}(w). \tag{8.3}$$

Thus, for the non-singlet case the logarithmic derivative of the Mellin transform of an FF is proportional to the Mellin transform of a splitting function, *independent of energy scale* (in LO). That result motivates a similar approach to the FFs themselves.

We multiply Eq. (8.1) by $x\ln(s/m_0^2)/xD(x,s)$. What remains on the RHS is the convolution integral, including splitting function $zP(z) = P(\zeta)$ with $\zeta = \ln(1/z)$ and fragmentation-function ratio $D_a(\xi-\zeta,s)/D_b(\xi,s)$. We then use the following transformations: $\xi \to y_{max} - y$, $\zeta \to y_{max} - y'$, $D(\xi) \to D(y_{max}-\xi) \sim D(y)$ and $D(\xi-\zeta) \to D(y_{max}-\xi+\zeta) \sim D(y+y_{max}-y')$, to obtain

$$\frac{d\ln D_b(y,y_{max})}{d\ln y_{max}} = \frac{1}{\pi A}\sum_a \int_y^{y_{max}} dy'\, P_{ab}(y_{max}-y')\,\frac{D_a(y+y_{max}-y',y_{max})}{D_b(y,y_{max})}, \tag{8.4}$$

an alternative form of the DGLAP equations on (y,y_{max}).

In Fig. 6 (third panel) we plot $d\ln D(y,y_{max})/d\ln y_{max}$ *vs* y_{max} for quark (solid) and gluon (dashed) FFs using the parameterized $D(y,y_{max})$ from Fig. 4 (fourth panel) for each parton type. There are three main features of the distributions: 1) nearly horizontal linear trends at larger energy scales (to the right of the dotted line), 2) ‘singularities’ at smaller energy scales due to kinematic boundaries and 3) minima at intermediate energies corresponding to a transition from ‘small’ (1-2) to ‘large’ (3 or more) fragment number, which may also relate to the emergence of parton color (quark-gluon distinction) at $Q \sim 8$ GeV. This form of the DGLAP equations eliminates the scale dependence of factor α_s and approximately cancels the scale dependence of the FFs in the ratio. In the perturbative region above $y_{max} = 5$ ($Q = 20$ GeV) the RHS is then dominated by the splitting function and nearly independent of energy scale, as with the Mellin transform version.

In Fig. 6 (fourth panel) $d\ln D(y,y_{max})/d\ln y_{max}$ *vs* $x_E = \cosh(y)/\cosh(y_{max})$ is plotted for quarks and gluons. In the limit $x_E \to 1$ ($y \to y_{max}$) and large y_{max} we expect [37]

$$\frac{\{d\ln D(y,y_{max})/d\ln y_{max}\}_{\text{gluon}}}{\{d\ln D(y,y_{max})/d\ln y_{max}\}_{\text{quark}}} \to \frac{C_A}{C_F} = 2.25. \tag{8.5}$$

The dotted lines are $a(x_E + b)$ and $2.25 \times a(x_E + b)$, with $a = -1.8$ and $b = 0.35$ adjusted to best match the quark points. The ratio trend is in reasonable agreement with the QCD expectation above $x_E = 0.2$.

9. Discussion

Our goal has been phenomenological extrapolation of e^+-e^- FFs to low Q^2 where the perturbative description of QCD is not applicable. Parton scattering and fragmentation at low Q^2 are in turn important for understanding the role of minijets in p-p and A-A collisions at RHIC. The beta distribution provides a simple but precise description of all measured FFs and accomplishes the desired extrapolation, but also reveals some interesting new aspects of parton fragmentation.

$\beta(u;p,q)$ describes systems in which entropy is maximized (*e.g.,* by a parton cascade) on a bounded interval (*e.g.,* bounded by the leading-parton momentum). The beta distribution maximizes the Shannon entropy $S = -\int dx\, p(x) \ln[p(x)]$ subject to constraints on geometric means $\overline{\ln(x)} = \int dx\, p(x)\, \ln(x)$ and $\overline{\ln(1-x)}$ (parameters of the splitting functions) [43]. Fragmentation of light quarks and gluons can thus be viewed as an equilibration process controlled by two opposing tendencies: parton splitting as a form of downscale energy transport which increases entropy and gluon coherence which constrains the splitting at a scale conjugate to hadron size. The observed fragment distribution is then a maximum-entropy configuration balancing those two tendencies.

Conventional scaling-violation systematics are easily and precisely reproduced by our parameterization over a broad energy range, as demonstrated down to kinematic limits in Fig. 6 (first panel). It is straightforward to explore the consequences of varying (p,q) energy trends. For example, Fig. 6 (fourth panel) demonstrates that the C_A/C_F limit for logarithmic derivatives previously established by specific experimental measurements (*e.g.,* [37, 40, 44, 45]) is consistent with the (p,q) parameterization determined by the present study.

10. Conclusions

Low-Q^2 parton collisions play a dominant role in nuclear collisions at RHIC. Little was known about low-Q^2 parton scattering and fragmentation prior to this work, and there exists little theoretical support for our experimental results in nuclear collisions. We therefore sought a phenomenological description by extrapolating energy trends of e^+-e^- fragmentation functions. We find that FFs plotted on rapidity y vary with energy in a nearly self-similar manner. FFs transformed to u are well described by a product of the dijet multiplicity and a unit-normal form factor modeled by the beta distribution. The latter is determined by parameters (p,q) which exhibit modest linear variations within perturbative energy scale range $Q > 20$ GeV. The beta distribution shape, when combined with an energy-conservation sum rule, also determines FF multiplicities. The factored representation on u thus provides a simple and compact representation of e^+-e^- FFs over a broad energy range and permits extrapolation to small energy scales.

In this analysis we have described all measured e^+-e^- fragmentation functions with a precise (few percent) model function. The model function (beta distribution) allows us to extrapolate fragmentation trends to low Q^2, to a kinematic region not accessed by conventional methods. Such low-Q^2 extrapolation provides a phenomenological context for minijet-related two-particle correlations in p-p and A-A collisions at RHIC, forming a basis for theoretical treatments of in-medium dissipation of low-Q^2 partons and the subsequent hadronization process in heavy ion collisions.

This work was supported in part by the Office of Science of the U.S. DoE under grant DE-FG03-97ER41020.

References

[1] T. A. Trainor (STAR Collaboration), Proceedings of the International Symposium on Multiparticle Dynamics (ISMD 2005), Kromĕříž, CR, August 9-15, 2005, Published in AIP Conf. Proc. **828**, 238 (2006).

[2] J. Adams et al. (STAR Collaboration), nucl-ex/0411003, to be published in Phys. Rev. C.

[3] J. Adams et al. (STAR Collaboration), nucl-ex/0408012.

[4] D. J. Prindle and T. A. Trainor, Proceedings of the MIT Workshop on Correlations and Fluctuations in Relativistic Nuclear Collisions, Cambridge, Massachusetts, 21-23 April 2005, J. Phys.: Conference series **27**, 118 (2005).

[5] Q. J. Liu, D. J. Prindle and T. A. Trainor, Phys. Lett. B, **632** 197 (2006).

[6] J. Adams et al. (STAR Collaboration), J. Phys. G. **32**, L37 (2006).

[7] J. Adams *et al.* (STAR Collaboration), Phys. Rev. D **74**, 032006 (2006).

[8] T. A. Trainor and D. J. Prindle (STAR Collaboration), *ibid*, p. 134.

[9] R. Jefferson Porter and Thomas A. Trainor (STAR Collaboration), *ibid*, p. 98.

[10] T. A. Trainor, R. J. Porter and D. J. Prindle J. Phys. G, **31**, 809-824 (2005).

[11] R. J. Porter and T. A. Trainor (STAR collaboration), hep-ph/0406330.

[12] R. J. Porter and T. A. Trainor (STAR Collaboration) *Acta Phys. Polon.* B, **36**, 353-359 (2005).

[13] T. A. Trainor and D. T. Kettler, Phys. Rev. D **74**, 034012 (2006).

[14] V. N. Gribov and L. N. Lipatov, Sov. J. Nucl. Phys. **15**, 438 (1972); L. N. Lipatov, Sov. J. Nucl. Phys. **20**, 95 (1975); Yu. L. Dokshitzer, Sov. Phys. JETP **46**, 641 (1977).

[15] G. Altarelli and G. Parisi, Nucl. Phys. B **126** , 298 (1977).

[16] M. Z. Akrawy et al. (OPAL Collaboration) Phys. Lett. B, **247**, 617 (1990).

[17] Yu. L. Dokshitzer, V. S. Fadin and V. A. Khoze, Phys. Lett. B **115**, 242 (1982).

[18] W. Braunschweig *et al.* (TASSO Collaboration), Z. Phys. C **47**, 187 (1990).

[19] B. R. Webber, J. Phys. G **17**, 1579 (1991).

[20] B. A. Kniehl, G. Kramer and B. Pötter, Nucl. Phys. B **582**, 514 (2000)

[21] P. Dahlqvist, B. Andersson, G. Gustafson, Nucl. Phys. B **328**, 76 (1989); B. Andersson, G. Gustafson, J. Samuelsson, Nucl. Phys. B **463**, 217 (1996).

[22] Yu. L. Dokshitzer, V. A. Khoze, A. H. Mueller and S. I. Troyan, *Basics of perturbative QCD*, Editions Frontières, Gif-sur-Yvette, 1991.

[23] H. Albrecht *et al.* (ARGUS Collaboration), Z. Phys. C **44**, 547 (1989).

[24] D. Buskulic *et al.* (ALEPH Collaboration), Z. Phys. C **66**, 355 (1995).

[25] A. Heister *et al.* (ALEPH Collaboration) Phys. Lett. B **512**, 30 (2001).

[26] D. Bortoletto *et al.* (CLEO Collaboration) Phys. Rev. D **37**, 1719 (1988); H. Albrecht *et al.* (ARGUS Collaboration) Z. Phys. C **52**, 353 (1991).

[27] C. Peterson, D. Schlatter, I. Schmitt and P. M. Zerwas, Phys. Rev. D **27**, 105 (1983).

[28] O. Biebel, P. Nason and B. R. Webber, "Jet fragmentation in e+ e- annihilation," hep-ph/0109282.

[29] D. Acosta *et al.* (CDF Collaboration), Phys. Rev. Lett. **94**, 171802 (2005).

[30] M. S. Alam *et al.* (CLEO Collaboration), Phys. Rev. D **56**, 17 (1997).

[31] G. Abbiendi *et al.* (OPAL Collaboration), Phys. Rev. D **69**, 032002 (2004).

[32] K. Ackerstaff *et al.* (OPAL Collaboration), Eur. Phys. J. C **1**, 479 (1996).

[33] I. M. Dremin and J. W. Gary, Phys. Rept. **349**, 301 (2001).

[34] H. Aihara *et al.* (TPC/Two Gamma Collaboration), Phys. Rev. Lett. **61**, 1263 (1988).

[35] C. P. Fong and B. R. Webber, Nucl. Phys. B **355**, 54 (1991).

[36] C. P. Fong and B. R. Webber, Phys. Lett. B **229**, 289 (1989).

[37] P. Abreu *et al.* (DELPHI Collaboration), Eur. Phys. J. C **13**, 573 (2000).

[38] M. Schmelling, "Status of the strong coupling constant," Talk given at 28th International Conference on High-energy Physics (ICHEP 96), Warsaw, Poland, 25-31 Jul 1996. Published in ICHEP 96:91-102 (QCD161:H51:1996), hep-ex/9701002.

[39] S. Albino, B. A. Kniehl, G. Kramer and W. Ochs, Phys. Rev. D **73**, 054020 (2006).

[40] G. Abbiendi *et al.* (OPAL Collaboration), Eur. Phys. J. C **37**, 25 (2004)

[41] D. J. Gross and F. Wilczek, Phys. Rev. D **9**, 980 (1974).

[42] H. Georgi and H. D. Politzer, Phys. Rev. D **9**, 416 (1974).

[43] J. N. Kapur and H. K. Kesavan, "Entropy Optimization Principles with Applications," Academic Press, San Diego, 1992.

[44] G. Abbiendi *et al.* (OPAL Collaboration), Eur. Phys. J. C **23**, 597 (2002).

[45] P. Abreu *et al.* (DELPHI Collaboration), Phys. Lett. B **449**, 383 (1999).